JOC The Journal of Organic Chemistry

Article

pubs.acs.org/joc

Stable Radical Cations and Their π-Dimers Prepared from Ethylene- and Propylene-3,4-dioxythiophene Co-oligomers: Combined Experimental and Theoretical Investigations

Tohru Nishinaga* and Yusuke Sotome

Department of Chemistry, Graduate School of Science and Engineering, Tokyo Metropolitan University, Hachioji, Tokyo 192-0397, Japan

Supporting Information

ABSTRACT: Co-oligomers composed of two 3,4-ethylenedioxythiophene (EDOT) units and two or three 3,4-propylenedioxythiophene (ProDOT) units, i.e., **2E2P$_{Et}$** and **2E3P$_{Et}$**, were newly synthesized together with the ProDOT trimer **3P$_{Me}$**. On the basis of cyclic voltammetry, the gaps between the first and second oxidation potentials (ΔE^{1-2}) of **2E2P$_{Et}$** and **2E3P$_{Et}$** were found to be larger than that of the previously synthesized ProDOT tetramer **4P$_{Hex}$**. These co-oligomers gave the fairly stable radical cations **2E2P$_{Et}$**$^{\bullet+}$ and **2E3P$_{Et}$**$^{\bullet+}$ by chemical oxidation with $AgSbF_6$. The disproportionation of **2E2P$_{Et}$**$^{\bullet+}$ and **2E3P$_{Et}$**$^{\bullet+}$ into neutral and dicationic species, which was observed for **4P$_{Hex}$**$^{\bullet+}$, was inhibited in accord with the larger ΔE^{1-2}. Additionally, the formation of the π-dimers $(\mathbf{3P_{Me}})_2^{2+}$, $(\mathbf{2E2P_{Et}})_2^{2+}$, and $(\mathbf{2E3P_E})_2^{2+}$ was clearly observed in dichloromethane solution at low temperatures with UV−vis−NIR spectroscopy. Furthermore, the π-dimerization enthalpies of **2E2P$_{Et}$**$^{\bullet+}$ and **2E3P$_{Et}$**$^{\bullet+}$ were greater than that of **3P$_{Me}$**$^{\bullet+}$, suggesting the formation of fully π-contacted structures. The structures of the π-dimers were optimized at the B97D3 method, and the calculated absorption spectra of the π-dimers obtained using TD-DFT methods were in reasonable agreement with the observed ones, supporting the reliability of the calculated structures.

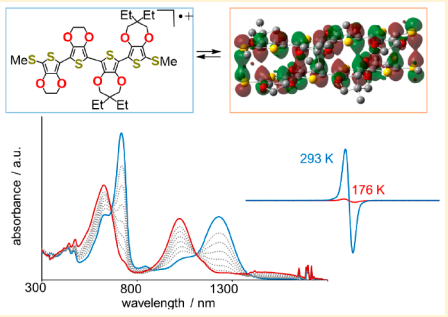

INTRODUCTION

In recent years, interest in self-associated π-dimers of stable ion radicals generated by redox reactions has been growing.[1−4] As an emerging intermolecular force, π-dimerization has been applied to the control of intramolecular motion[1] and the construction of various supramolecular structures.[2] Thus far, bipyridinium[5−11] and tetrathiafulvalene (TTF)[12−14] have played a central role in the π-dimer-based supramolecular chemistry, although oligothiophenes[15−18] and other π-systems[1,19] have been occasionally utilized. However, oligothiophenes might not necessarily be suitable for these purposes because the radical cations are insufficiently stable in the condensed phase without appropriate structural modifications.[4]

Initially, the π-dimerization of the oligothiophene radical cation was demonstrated in relation to the conduction mechanism of polythiophenes.[20] In the first study, methyl end-capped terthiophene was used, but the radical cation was found to be labile.[21] Since then, various oligothiophenes have been designed and synthesized as models of p-doped polythiophenes to further investigate the electronic structures of the π-dimers of oligothiophene radical cations.[15,22−36] Among them, the oligomers of 3,4-ethylenedioxythiophene (EDOT)[37−41] are considered to be particularly interesting, because the polymer of EDOT (PEDOT) is the most successful conducting polymer.[42] Nevertheless, the low solubility of EDOT oligomers and their oxidized states limit the synthesis of longer oligomers, and, hence, the detailed investigations of their oxidized states. From the perspective of the stability of the radical cations, the electron donating 3,4-dioxy substituents are quite attractive.

The solubility problem associated with EDOT oligomers can be avoided if 3,4-propylenedioxythiophene (ProDOT)[43] with appropriate alkyl groups on the center of the propylene bridge is used instead. Thus, in the previous study, we synthesized oligomers ***n*P$_{Hex}$** (up to the dodecamer) composed of ProDOT with di-*n*-hexyl groups (ProDOT-Hex) and bis(methylthio) end-capping units and observed the multielectron oxidation states (up to the hexacation of **12P$_{Hex}$**).[44] However, in terms of the π-dimerization of radical cations, even **4P$_{Hex}$**$^{\bullet+}$ showed not only π-dimerization but also simultaneous disproportionation into neutral and dicationic species as the temperature of the dilute CH_2Cl_2 solution was lowered. Furthermore, under similar conditions, the longer ***n*P$_{Hex}$** only exhibited disproportionation. These results indicate that ProDOT tetramers and longer oligomers are not suitable for π-dimer-based supramolecular chemistry, despite the high stability of their oxidized states.

In the present study, we investigated the stability and π-dimerization ability of radical cations of the shorter ProDOT trimer **3P$_{Me}$** and co-oligomers composed of EDOT and ProDOT units **2E2P$_{Et}$** and **2E3P$_{Et}$**. These oligomers were

Received: April 7, 2017
Published: June 26, 2017

DOI: 10.1021/acs.joc.7b00816
J. Org. Chem. 2017, 82, 7245−7253

end-capped with bis(methylthio) groups, as in our previous studies, to prevent the radical coupling that causes these oligomers to polymerize. We found that **2E2P$_{Et}$** and **2E3P$_{Et}$** gave fairly stable radical cations that formed π-dimers in CH_2Cl_2 solution at low temperatures. Herein, we analyze the π-dimerization ability of these radical cations in terms of the thermodynamic parameters obtained via variable-temperature UV−vis−NIR spectroscopy. We also discuss the electronic structures of these radical cation π-dimers based on the combined experimental and theoretical results.

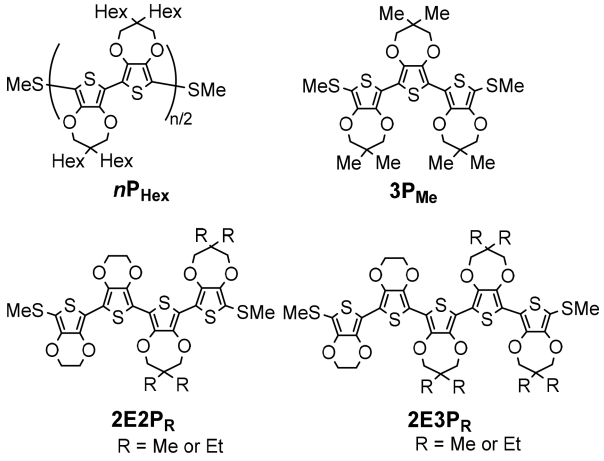

RESULTS AND DISCUSSION

Synthesis. As shown in Scheme 1, the methylthio derivative of ProDOT-Me **1** was obtained by lithiation with *n*-butyl lithium, followed by reaction with dimethyldisulfide. Then, **1** was stannylated and subjected to double Stille coupling with diiodo-ProDOT-Me **2** obtained by iodination with *N*-iodosuccinimide (NIS) to give **3P$_{Me}$**. In a preliminary test, we also attempted to synthesize methylthio-end-capped EDOT trimer using the same method, but the low solubility of the products hampered the purification process.

For EDOT-ProDOT co-oligomers, we first tried to synthesize tetramers composed of three or two EDOT units and one or two ProDOT-Me unit(s). However, studying π-dimerization with these oligomers was found to be difficult because of their low solubility in both neutral and oxidized states. In particular, the solubility of the oxidized oligomer with three EDOT units was considerably low. Thus, two and three ProDOT-Et units were introduced to form a co-tetramer and co-pentamer, respectively. Both the EDOT dimer and ProDOT-Et dimer were capped with methylthio groups. The resultant **3** was stannylated, whereas **4** was iodinated. Stille coupling of the stannane and iodide gave **2E2P$_{Et}$**. Similarly, **2E3P$_{Et}$** was synthesized using mono-methylthio capped ProDOT-Et trimer **5**.

Redox Behavior. Next, the electrochemical behaviors of the ProDOT-Me trimer **3P$_{Me}$** and the EDOT−ProDOT-Et co-oligomers **2E2P$_{Et}$** and **2E3P$_{Et}$** were investigated with cyclic voltammetry. As shown in Figure 1 and Table 1, these

Scheme 1. Synthesis of 3P$_{Me}$, 2E2P$_{Et}$, and 2E3P$_{Et}$

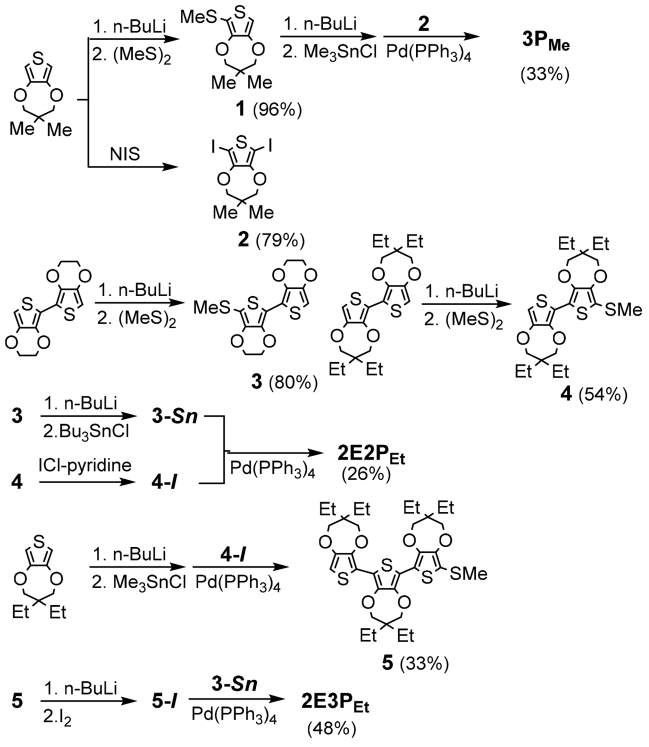

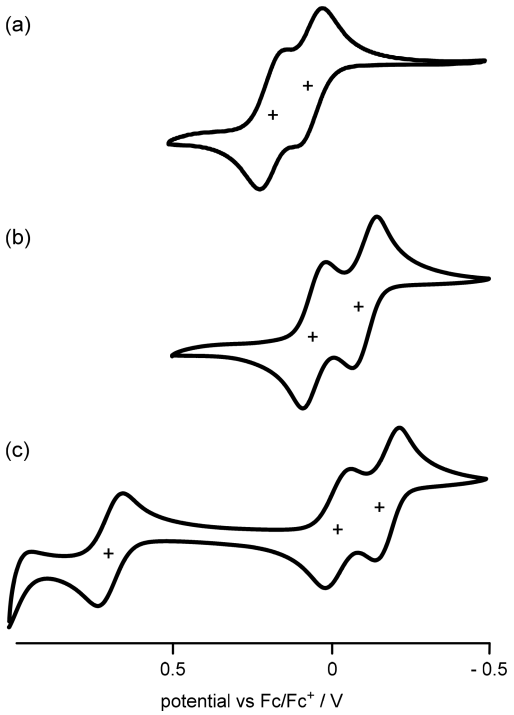

Figure 1. Cyclic voltammograms of (a) **3P$_{Me}$**, (b) **2E2P$_{Et}$**, and (c) **2E3P$_{Et}$**.

Table 1. Oxidation Potentials (E^{ox}) and Gap between First and Second Oxidation Potentials (ΔE^{1-2}) of 3P$_{Me}$, 2E2P$_{Et}$, and 2E3P$_{Et}$[a]

compd	$E_{1/2}^{ox1}$/V[b]	$E_{1/2}^{ox2}$/V[b]	$E_{1/2}^{ox3}$/V[b]	ΔE^{1-2}/V
3P$_{Me}$	+0.04	+0.16		0.12
4P$_{Hex}$[c]	−0.05	+0.04		0.09
2E2P$_{Et}$	−0.11	+0.05		0.16
2E3P$_{Et}$	−0.17	−0.02	+0.70	0.15

[a]Conditions: 1 mM in CH_2Cl_2 with 0.1 M Bu_4NPF_6. [b]Potentials vs Fc/Fc^+. [c]Reference 44.

DOI: 10.1021/acs.joc.7b00816
J. Org. Chem. 2017, 82, 7245−7253

(co)oligomers showed multiple one-electron oxidation steps and all the steps were found to be reversible in CH_2Cl_2 with 0.1 M tetra-*n*-butylammonium hexafluorophosphate. In our previous study, the gap between the first and second oxidation potentials (ΔE^{1-2}) was narrow (0.09 V) for $\mathbf{4P_{Hex}}$, and zero for $\mathbf{6P_{Hex}}$ and the longer oligomers.[44] Thus, the disproportionation of radical cation $\mathbf{4P_{Hex}}^{\bullet+}$ into neutral and dicationic species was observed because of the small ΔE^{1-2}. In contrast, ΔE^{1-2} of $\mathbf{3P_{Me}}$ (0.12 V) was larger than that of $\mathbf{4P_{Hex}}$, because the second oxidation in the smaller π-system caused larger Coulombic repulsion. In contrast, $\mathbf{2E2P_{Et}}$ and even $\mathbf{2E3P_{Et}}$ were also found to have larger ΔE^{1-2} than $\mathbf{3P_{Me}}$, even though these co-oligomers have larger π-systems. Comparing the oxidation potentials of the tetramers revealed that the first oxidation potential of the mixed tetramer $\mathbf{2E2P_{Et}}$ (−0.11 V vs Fc/Fc^+) was lower than that of $\mathbf{4P_{Hex}}$ (−0.05 V vs Fc/Fc^+), whereas the second oxidation potential of $\mathbf{2E2P_{Et}}$ (+0.05 V vs Fc/Fc^+) was similar to that of $\mathbf{4P_{Hex}}$ (+0.04 V vs Fc/Fc^+).

The lower first and similar second oxidation potentials of $\mathbf{2E2P_{Et}}$ relative to $\mathbf{4P_{Hex}}$ can be rationalized by the alteration in the donor abilities of EDOT and ProDOT in neutral and radical cation states. In the neutral state, the HOMO level of EDOT (B3LYP/6-31G(d)) was calculated to be 0.21 eV higher than that of ProDOT-H (Figure S1a in the Supporting Information), indicating that neutral EDOT has stronger donor ability. In contrast, the ProDOT radical cation was shown to have a higher SOMO level than the EDOT radical cation at the same level of theory (Figure S1b), suggesting that ProDOT radical cation has similar or even better donor ability than the EDOT radical cation. These alterations are believed to be attributable to conformational changes around the oxygen atoms before and after one-electron oxidation. The electron donation by the lone-pair of the oxygen atoms in neutral ProDOT appears to be less favorable because of the conformational mismatch between the oxygen p-orbitals containing the lone-pair and the thiophene p-orbitals, whereas the p-orbitals become nearly parallel to each other after one-electron oxidation because of the probable resonance structure with double bond character in the C−O bond (Figure S1c). Thus, the replacement of a ProDOT unit with an EDOT unit in these oligomers mainly decreased the first oxidation potential. As a result, the ΔE^{1-2} values of $\mathbf{2E2P_{Et}}$ and $\mathbf{2E3P_{Et}}$ became larger than that of $\mathbf{4P_{Hex}}$. Larger ΔE^{1-2} values are expected to inhibit the disproportionation of radical cation species into neutral and dicationic species, which is necessary for the realization of π-dimerization using 3,4-dioxythiophene oligomer radical cations.

Chemical Oxidation and π-Dimerization. Chemical one-electron oxidations of the oligomers prepared in this study were performed with silver hexafluoroantimonate ($AgSbF_6$) in CH_2Cl_2 solution (Scheme 2), and the reaction was monitored with UV−vis−NIR and ESR spectra. As shown in Figure 2, the reaction of $\mathbf{3P_{Me}}$, $\mathbf{2E2P_{Et}}$, and $\mathbf{2E3P_{Et}}$ with 1 equiv of $AgSbF_6$ at room temperature caused the characteristic changes in the absorption spectra corresponding to the formation of radical cation monomers. The observed absorption maxima are summarized in Table 2. The two absorption bands with contributions from HOMO−SOMO and SOMO−LUMO transitions (see below) were observed for the radical cations. The bathochromic shifts of each band as the oligomer lengths increased were also recorded.

Scheme 2. One-Electron Oxidation of $\mathbf{3P_{Me}}$, $\mathbf{2E2P_{Et}}$, and $\mathbf{2E3P_{Et}}$ and π-Dimerization of the Generated Radical Cations

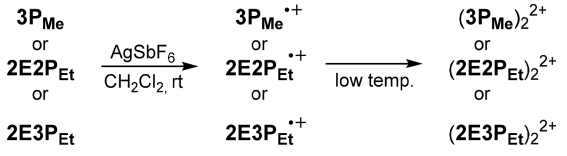

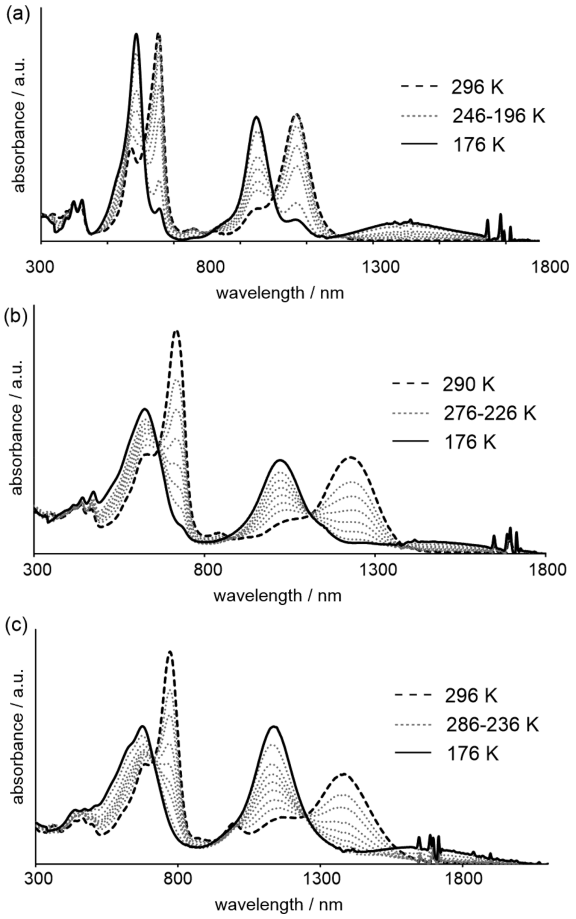

Figure 2. UV−vis−NIR spectra of (a) $\mathbf{3P_{Me}}^{\bullet+}$ (2.2×10^{-4} M), (b) $\mathbf{2E2P_{Et}}^{\bullet+}$ (2.6×10^{-4} M), and (c) $\mathbf{2E3P_{Et}}^{\bullet+}$ (1.5×10^{-4} M) in CH_2Cl_2 at various temperatures.

Table 2. Observed and Calculated Absorption Bands (λ) of the Radical Cations $\mathbf{3P_{Me}}^{\bullet+}$, $\mathbf{2E2P_R}^{\bullet+}$, and $\mathbf{2E3P_R}^{\bullet+}$ and Their π-Dimers

	radical cation		π-dimer	
compd	λ_{obs}/nm	λ_{calc}/nm[a,b]	λ_{obs}/nm	λ_{calc}/nm[a,b]
$\mathbf{3P_{Me}}^{\bullet+}$	1068, 654	1042, 615	~1410, 948, 587	1302, 984, 571
$\mathbf{2E2P_R}^{\bullet+c}$	1228, 717	1245, 753, 718, 670	~1470, 1021, 624	1481, 1192, 666, 629
$\mathbf{2E3P_R}^{\bullet+c}$	1384, 772	1456, 830, 803, 745	~1650, 1138, 676	1685, 1396, 788, 748, 658

[a]Calculated at the TD-B97D3/6-31G(d)//B97D3/6-31G(d) level with PCM (CH_2Cl_2). [b]Selected bands with oscillator strength $f > 0.1$. [c]R = Et for observation and R = Me for calculations.

The stability of $\mathbf{3P_{Me}}^{\bullet+}$, $\mathbf{2E2P_{Et}}^{\bullet+}$, and $\mathbf{2E3P_{Et}}^{\bullet+}$ was monitored by collecting the absorption spectra of CH_2Cl_2

DOI: 10.1021/acs.joc.7b00816
J. Org. Chem. 2017, 82, 7245−7253

solutions at room temperature under air in a quartz cell with a cap. The absorbances of $\mathbf{2E2P_{Et}}^{\bullet+}$ and $\mathbf{2E3P_{Et}}^{\bullet+}$ did not change over more than 3 h, whereas that of $\mathbf{3P_{Me}}^{\bullet+}$ decreased slightly (11% in 3 h) (Figure S2 in the Supporting Information). Thus, the radical cations $\mathbf{2E2P_{Et}}^{\bullet+}$ and $\mathbf{2E3P_{Et}}^{\bullet+}$ are fairly stable, although $\mathbf{3P_{Me}}^{\bullet+}$, which has the shorter oligomer length, was less stable than the longer ones. A highly stable radical cation state is favorable for supramolecular chemistry applications of these oligomers.

Next, the π-dimer formations of $\mathbf{3P_{Me}}^{\bullet+}$, $\mathbf{2E2P_{Et}}^{\bullet+}$, and $\mathbf{2E3P_{Et}}^{\bullet+}$ were investigated with variable-temperature (VT) UV−vis−NIR spectra. As the temperature of the CH_2Cl_2 solutions of $\mathbf{3P_{Me}}^{\bullet+}$, $\mathbf{2E2P_{Et}}^{\bullet+}$, and $\mathbf{2E3P_{Et}}^{\bullet+}$ was lowered, the characteristic change in the absorption spectra corresponding to π-dimer formation was clearly observed (Figure 2). The absorption maxima of the π-dimers $(\mathbf{3P_{Me}})_2^{2+}$, $(\mathbf{2E2P_{Et}})_2^{2+}$, and $(\mathbf{2E3P_{Et}})_2^{2+}$ are also summarized in Table 2. In all of the absorption spectra of the π-dimers, a broad absorption band attributed to the HOMO−LUMO transition of the π-dimer (see below) was observed in longer wavelength regions. In addition, the original absorption bands of the monomer radical cations were hypsochromically shifted. These spectral changes are typically observed during the π-dimerization of oligothiophene radical cations with medium length,[22,23,35,45] and the structures of the π-dimers were considered to be closely related to each other. Furthermore, ESR spectra of $\mathbf{3P_{Me}}^{\bullet+}$, $\mathbf{2E2P_{Et}}^{\bullet+}$, and $\mathbf{2E3P_{Et}}^{\bullet+}$ collected at room temperature confirmed the presence of radical species. For $\mathbf{3P_{Me}}^{\bullet+}$, the observed hyperfine coupling ($a_H \sim 1.4$ G) is ascribed to the end-capping methylthio groups based on the averaged coupling constants of methyl hydrogens ($a_H = 1.3$ G) calculated at the UB97D3/6-31G(d) level. In contrast, the signal intensity decreased significantly at low temperatures as shown in Figure 3. These results also supported the formation of π-dimers.

The VT absorption spectra contained the isosbestic points. Thus, π-dimer formation was considered to be the only ongoing reaction as the temperature was lowered. On the basis of the changes in the second absorption bands (600−800 nm) of the monomer radical cations, the equilibrium constant for the dimerization process at each temperature was estimated. Then, the thermodynamic parameters, (i.e., dimerization enthalpy ΔH_{dim} and entropy ΔS_{dim}) were obtained with a van't Hoff plot (Figure S3 in the Supporting Information). The results are summarized in Table 3.

The observed dimerization enthalpy ΔH_{dim} increased as the oligomer length increased, although the difference between the values was small and comparable to the experimental error. Nevertheless, the conclusion observed in various oligothiophenes that longer oligomers have greater π-dimerization abilities[22,35,45] is applicable to the present (co)oligomers, because, at similar concentrations, the dimerization processes of longer oligomers began at higher temperatures (see Figure 2).

The SOMO−SOMO interactions in π-dimers lead to the HOMOs and LUMOs in the π-dimers[35,46] (Figure 4), and the electrons are stabilized depending on the strength of these SOMO−SOMO interactions. Therefore, the HOMO−LUMO transition energy of the π-dimer should reflect the strength of the SOMO−SOMO interaction, which is one of the principal driving forces of π-dimerization.[35] However, as the HOMO−LUMO transition was shown to shift bathochromically with increasing length of the (co)oligomers, longer co-oligomers are thought to exhibit weaker stabilization energies. This would be due to the enhanced spin delocalization in longer oligomers which weakens the SOMO−SOMO interaction. In this context, it is interesting to note that the HOMO−LUMO transition energies of the present oligomers are lower than those of alkyl-oligothiophene radical cation π-dimers with the same numbers of thiophene units.[46] For example, the corresponding absorption band in quaterthiophene **6a** annelated with two bicyclo[2.2.2]octene units, which was also predicted to have an all-*trans* conformation of the neighboring thiophene units in the π-dimer, was observed at a shorter wavelength (1318 nm)[35]

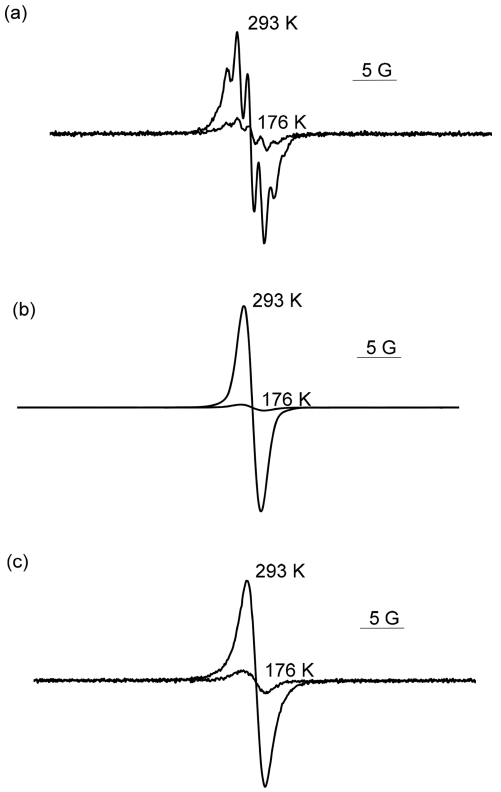

Figure 3. ESR spectra of (a) $\mathbf{3P_{Me}}^{\bullet+}$, (b) $\mathbf{2E2P_{Et}}^{\bullet+}$, and (c) $\mathbf{2E3P_{Et}}^{\bullet+}$ in CH_2Cl_2 at 293 and 176 K.

Table 3. Observed π-Dimerization Enthalpy (ΔH_{dim}) and Entropy (ΔS_{dim}) and Calculated π-Dimerization Energy (ΔE_{dim}) of $\mathbf{3P_{Me}}^{\bullet+}$, $\mathbf{2E2P_R}^{\bullet+}$, and $\mathbf{2E3P_R}^{\bullet+}$

compd	ΔH_{dim}[a]/ kcal mol^{-1}	ΔS_{dim}[a]/cal K^{-1} mol^{-1}	ΔE_{dim}[b]/ kcal mol^{-1}
$\mathbf{3P_{Me}}^{\bullet+}$	−10.8	−33	−51.2
$\mathbf{2E2P_R}^{\bullet+}$[c]	−11.4	−28	−60.4
$\mathbf{2E3P_R}^{\bullet+}$[c]	−11.7	−26	−73.4

[a]Experimental errors are within ±1 kcal mol^{-1} and ±6 cal K^{-1} mol^{-1}. [b]Calculated at the B97D3/6-31G(d) level with PCM (CH_2Cl_2) using the equation $\Delta E_{dim} = E_{\pi\text{-dimer}} - 2 \times E_{\text{radical cation}}$. [c]R = Et for observation and R = Me for calculations.

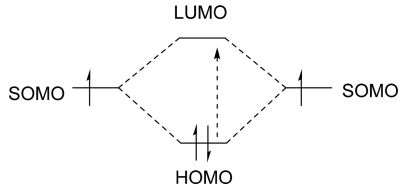

Figure 4. Schematic drawing of the SOMO−SOMO interaction.

DOI: 10.1021/acs.joc.7b00816
J. Org. Chem. 2017, 82, 7245−7253

than that of $(\mathbf{2E2P_{Et}})_2^{2+}$ (1470 nm). This result may also be attributed to the enhanced spin delocalization into the 3,4-dioxy parts of the present oligomer radical cations.

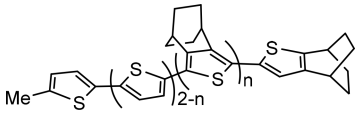

6a(n = 1), **6b**(n = 2)

The weaker SOMO−SOMO interactions in longer oligomers should be overbalanced by enhanced van der Waals interactions because of a possible wide contact between these longer molecules. Actually, in the previous study, no π-dimerization was observed for the quaterthiophene **6b** annelated with three bicyclo[2.2.2]octene units because of its limited contact area.[35] Thus, the increase of ΔH_{dim} with increasing (co)oligomer length suggested a fully (rather than partially) contacted structure of the π-dimers for $(\mathbf{2E2P_{Et}})_2^{2+}$ and $(\mathbf{2E3P_{Et}})_2^{2+}$.

On the other hand, the smaller ΔS_{dim} values of $\mathbf{2E2P_{Et}}^{\bullet+}$ and $\mathbf{2E3P_{Et}}^{\bullet+}$ relative to that of $\mathbf{3P_{Me}}^{\bullet+}$ may be caused by the inclusion of the sterically less hindered EDOT unit. Two methylene-oxy parts in the propylene dioxy moiety of ProDOT units stand up from the thiophene π-plane, because the resonance effect shown in Figure S1c is weakened in the wider π-system. This methylene part leads to greater steric repulsion during π-dimer formation when the methylene parts point inside the dimer structure (see Experimental Section in the Supporting Information). As a result, $(\mathbf{3P_{Me}})_2^{2+}$ may require a more restricted conformation of the propylene dioxy moiety to avoid preventing π-dimer formation.

DFT Calculations. Usually the structures of radical ion π-dimers cannot be fully optimized using the most popular DFT, i.e., the B3LYP method, when no dispersion or long-range corrections are combined. In our previous study, the M06-2X method was chosen for the calculations of the π-dimers of bicyclo[2.2.2]octane-annelated oligothiophenes[35] and dithienylpyrroles,[47] because M06-2X has improved performance for noncovalent interactions as compared with M06 and M06-L.[48] Therefore, in the present study, we again first conducted the geometry optimization of $(\mathbf{3P_{Me}})_2^{2+}$ at the UM06-2X/6-31G(d) level combined with the broken-symmetry (BS) approach and polarized continuum model (PCM) of CH_2Cl_2 solvation for the singlet diradicaloid model. In this case, the BS singlet state ($\langle S^2\rangle$ = 0.7881, Table 4) was found to be more stable than the closed shell singlet state (RM06-2X/6-31G(d)) by 2.38 kcal mol^{-1}. The diradical character of $(\mathbf{3P_{Me}})_2^{2+}$ at the BS-UM06-2X/6-31G(d) level estimated based on the LUMO occupation number in the natural population analysis[49] was 0.48. Next, time-dependent (TD) DFT calculations were employed to predict the absorption spectrum of $(\mathbf{3P_{Me}})_2^{2+}$ at the same level. However, the calculated absorption spectrum differed from the observed one (Figure 5). In particular, the longest absorption band in the π-dimer was too close to the next absorption band in the calculated spectrum. The M06-2X method is a hybrid DFT with 54% Hartree−Fock (HF) exchange, and recently hybrid DFT with high HF exchange was determined to result in large error in the TD-DFT calculations of radical ion dimers.[50]

Table 4. Intermolecular Nearest C−C, C−S, and S−S Distances and $\langle S^2\rangle$ Values before Annihilation in $(\mathbf{3P_{Me}})_2^{2+}$ Calculated at Various DFT with BS and PCM Methods and 6-31G(d) Basis Set

method	C−C/Å	C−S/Å	S−S/Å	$\langle S^2\rangle$
M06-2X	3.25[a]	3.34[b]	3.58[c]	0.7881
M06	3.402[d]	3.48[e]	3.73[c]	0.7586
M06-L	3.33[f]	3.39[b]	3.53[c]	0.0000
B97D3(BJ)	3.34[f]	3.41[b]	3.56[c]	0.0000

[a]Between the α-carbon and β-carbon in the central thiophene units. [b]Between the sulfur and β-carbon in the central thiophene units. [c]Between sulfur atoms in methylthio groups. [d]Between the α-carbons in the terminal thiophene units. [e]Between the sulfur and β-carbon in the terminal thiophene units. [f]Between the α-carbons in the central thiophene units.

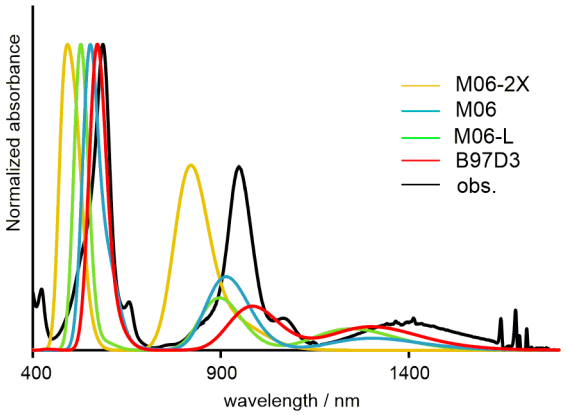

Figure 5. Calculated and observed UV−vis−NIR spectra of $(\mathbf{3P_{Me}})_2^{2+}$ (basis set: 6-31G(d)).

To study the dependencies of DFT methods, geometry optimizations of $(\mathbf{3P_{Me}})_2^{2+}$ were conducted using the recently recommended M06 (for calculations of sulfur-centered neutral radical dimers[51]) and B97D3(BJ) (for TTF or tetracyanoethylene (TCNE) radical ion dimers[52]) in addition to M06-L. The spectra calculated with these methods are also shown in Figure 5, one of the optimized structure (B97D3/6-31G(d)) is shown in Figure 6a, and the nearest C−C, C−S, and S−S contact distances and $\langle S^2\rangle$ values of the optimized structures are summarized in Table 4. M06 is also a hybrid DFT with 27% HF exchange, whereas B97D3 and M06-L are pure DFT methods. In the M06 structure ($\langle S^2\rangle$ = 0.7586), the diradical character was shown to be 0.48, whereas, in the B97D3 and M06-L structures, the closed-shell singlet dication was found to be the ground state ($\langle S^2\rangle$ = 0.0000) even with the BS method. These results do not conflict with the previous findings that pure DFT methods tend to avoid symmetry breaking, whereas hybrid DFT methods do not.[52,53] In the TD-DFT calculations, all of these methods indicated three absorption bands similar to the observed spectra. Comparing the calculated spectra revealed that M06 and B97D3 gave slightly better predictions than M06-L. In contrast, regarding the intermolecular distances, only M06 gave the nearest C−C and S−S distances that were longer than the sum of the van der Waals radii of carbon and sulfur (C−C: 3.4 Å; S−S: 3.6 Å) in the optimized structures. These results are in sharp contrast to the fact that many π-dimers of stable radicals have C−C or S−S distances shorter than the usual van der Waals contacts.[3,4] Therefore, we also concluded that, from the perspectives of the equilibrium structures and the prediction of the absorption spectra, the best compromise for calculations of the present (co)oligomer radical cation π-dimers is to use the B97D3(BJ) method. However, it

DOI: 10.1021/acs.joc.7b00816
J. Org. Chem. 2017, 82, 7245−7253

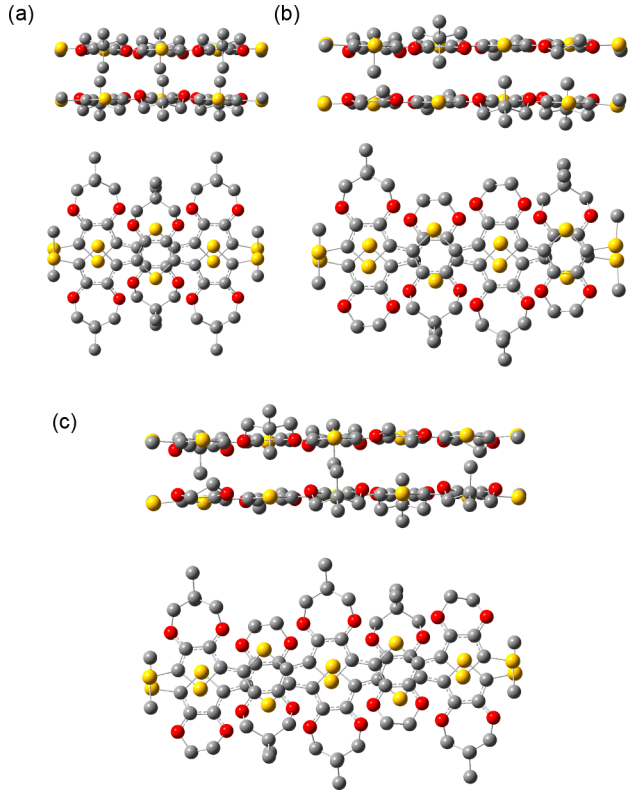

Figure 6. Side and top views of optimized structures of (a) $(\mathbf{3P_{Me}})_2^{2+}$, (b) $(\mathbf{2E2P_{Me}})_2^{2+}$, and (c) $(\mathbf{2E3P_{Me}})_2^{2+}$ at the B97D3/6-31G(d) level. Hydrogen atoms are omitted for clarity.

should be noted that judging the diradical character of these π-dimers remains difficult. Given that M06-2X provided a similar HOMO-occupation number with restricted active space self-consistent field (RASSCF) calculations for TTF and TCNE radical ion dimers,[52] the diradical character of $(\mathbf{3P_{Me}})_2^{2+}$ may also be similar to 0.48 as obtained by the M06-2X calculations despite no diradical character in the B97D3 structure.

The structure optimization of the π-dimers $(\mathbf{2E2P_{Me}})_2^{2+}$ and $(\mathbf{2E3P_{Me}})_2^{2+}$ and the monomer radical cations $\mathbf{3P_{Me}}^{\bullet+}$, $\mathbf{2E2P_{Me}}^{\bullet+}$, and $\mathbf{2E3P_{Me}}^{\bullet+}$, and their TD-DFT calculations were performed at the B97D3/6-31G(d) level with PCM. Here, we used the ProDOT-Me unit for the calculations of the co-oligomers. The structures of the π-dimers are shown in Figure 6, and the results of calculated absorption maxima are summarized in Table 2. As in the case for $(\mathbf{3P_{Me}})_2^{2+}$, the calculations of $(\mathbf{2E2P_{Me}})_2^{2+}$ and $(\mathbf{2E3P_{Me}})_2^{2+}$ at this level of theory with the BS method resulted in that the closed-shell singlet dication ($\langle S^2 \rangle$ = 0.0000) was the ground state. Additionally, the intermolecular nearest C−C and C−S distances were 3.36 and 3.42 Å for $(\mathbf{2E2P_{Me}})_2^{2+}$ and 3.39 and 3.45 Å for $(\mathbf{2E3P_{Me}})_2^{2+}$, respectively, whereas the S−S distances were slightly longer than the sum of the van der Waals radii of two sulfur atoms.

The calculated absorption spectra of the monomer radical cations $\mathbf{3P_{Me}}^{\bullet+}$, $\mathbf{2E2P_{Me}}^{\bullet+}$, and $\mathbf{2E3P_{Me}}^{\bullet+}$ mainly contained two absorption bands. For the longer absorption bands, the contribution of HOMO−SOMO transitions is the most important with configuration interaction (CI) coefficients ranging from 0.91 to 0.93 in the unrestricted calculations for the open-shell system. The next bands involved SOMO−LUMO transition (CI coefficients ranging from 0.60 to 0.82) with contributions of other various transitions. The mean deviation of the calculated HOMO−SOMO transition energies from the observed values was small (0.03 eV), whereas that of the next second bands was 0.1 eV. This larger mean deviation may stem from the contributions of various transitions to the second bands.

For $(\mathbf{2E2P_{Me}})_2^{2+}$ and $(\mathbf{2E3P_{Me}})_2^{2+}$, three main bands appeared in the calculated spectra, similar to those of $(\mathbf{3P_{Me}})_2^{2+}$. The longest absorption bands can be assigned as HOMO−LUMO transition of the π-dimers,[35,45] because the CI coefficients of the bands for all π-dimers were approximately 0.75 (with LUMO−HOMO contributions of ca. −0.25) in the restricted calculations for the closed-shell system. As shown in Figure S4 (in the Supporting Information), the HOMO and LUMO have characteristics of the bonding and antibonding orbitals derived from the SOMO−SOMO interactions of the corresponding radical cations. The calculated HOMO−LUMO transition energies reproduced the experimental values very well with a mean deviation of 0.03 eV. The other bands were also in reasonable agreement with the observed ones. Accordingly, it can be safely concluded that the B97D3 method is useful for predicting the structures of oligothiophene radical cation π-dimers as well as in the case of the TTF and TCNE radical ion dimers.

Finally, we calculated the dimerization energy with the PCM solvation model (Table 3). In our previous analysis, the change in the solvation upon the formation of radical cation π-dimers is an important driving force of π-dimerization, because the solvation energy of the π-dimer dication is more than twice that of the monomer radical cation.[35] The dimerization energy of the terthiophene radical cation calculated at the RM06-2X/6-31G(d) level was in good agreement with the observed ΔH_{dim}, whereas the calculations overestimated the dimerization energies of longer oligomers.[35] The differences increased with increasing oligomer length. For $\mathbf{3P_{Me}}^{\bullet+}$, the dimerization energy was calculated to be −31.2 kcal mol^{-1} at the BS-UM06-2X/6-31G(d) level, which was quite different from the observed ΔH_{dim} (−10.8 kcal mol^{-1}). This large difference is not caused by the inclusion or omission of the BS method, because the energy difference between the restricted and unrestricted models of $(\mathbf{3P_{Me}})_2^{2+}$ was only 2.38 kcal mol^{-1}. Similarly, the calculated dimerization energies for $\mathbf{3P_{Me}}^{\bullet+}$, $\mathbf{2E2P_{Me}}^{\bullet+}$, and $\mathbf{2E3P_{Me}}^{\bullet+}$ calculated at the B97D3/6-31G(d) level with PCM were shown to be much larger than the corresponding ΔH_{dim} values. The attribution of the errors in the calculations is not simple, but overestimating the van der Waals forces in larger π-systems and/or ignoring the effect of the counteranion are possibilities.

CONCLUSION

In the present study, we synthesized new co-oligomers composed of EDOT and ProDOT units $\mathbf{2E2P_{Et}}$ and $\mathbf{2E3P_{Et}}$ and the ProDOT trimer $\mathbf{3P_{Me}}$. Electrochemical measurements revealed that the combination of EDOT units and ProDOT units lowered only the first oxidation potentials of the 3,4-dioxythiophene oligomers. As a result, $\mathbf{2E2P_{Et}}$ and $\mathbf{2E3P_{Et}}$ had the relatively large ΔE^{1-2} values, which inhibited the disproportionation of the radical cation into neutral and radical cation species. The radical cations $\mathbf{2E2P_{Et}}^{\bullet+}$ and $\mathbf{2E3P_{Et}}^{\bullet+}$ generated with $AgSbF_6$ were shown to have sufficient solubility with high stability at room temperature under air, which formed π-dimers $(\mathbf{2E2P_{Et}})_2^{2+}$, and $(\mathbf{2E3P_{Et}})_2^{2+}$ in CH_2Cl_2 solution at low temperatures. These properties cannot be attained without

DOI: 10.1021/acs.joc.7b00816
J. Org. Chem. 2017, 82, 7245−7253

mixing the EDOT and ProDOT units, because low solubility hampered the purification of EDOT trimer end-capped with methylthio groups or tetramer with phenyl groups,[38] and because radical cations of the ProDOT tetramer or longer oligomers showed disproportionation rather than π-dimerization.[44] The observed absorption bands of the π-dimers were reproduced very well at the TD-B97D3/6-31G(d)//BS-UB97D3/6-31G(d) level, indicating the reliability of the structures at this level of theory. In conclusion, we successfully synthesized new oligothiophene radical cations with sufficient solubility, high stability, and π-dimerization ability. These EDOT and ProDOT co-oligomers are potentially useful supramolecular synthons, e.g., for the construction of supramolecular conducting wires based on the selective π-dimer formations of radical cation moieties. Further research along these lines is now under way.

EXPERIMENTAL SECTION

General. ^{1}H and ^{13}C NMR spectra were recorded on Bruker AV500 or JEOL JNM-270 instruments. Chemical shifts are reported in ppm with reference to tetramethylsilane, using the signal of internal tetramethylsilane or the solvents. APCI mass spectra were recorded on a Bruker MicrOTOFII-SD. Only the more intense or structurally diagnostic mass spectral fragment ion peaks are reported. Electronic absorption spectra were recorded on a SHIMADZU UV−vis−NIR scanning spectrophotometer (Model UV-3101-PC). Variable-temperature measurements of electronic absorption spectra were performed using an Oxford Optistat DN liquid-nitrogen cryostat. Cyclic voltammetry (CV) was performed on a BAS-ALS620B electrochemical analyzer using a standard three-electrode cell consisting of a Pt disk working electrode, a Pt wire counter electrode, and a Ag/AgCl reference electrode under a nitrogen atmosphere. The potentials were calibrated with ferrocene as an internal standard. ESR spectra were recorded on a Bruker E500 instrument. Preparative gel-permeation chromatography (GPC) was performed with a JAI LC-08 chromatograph equipped with JAIGEL 1H and 2H columns.

Commercially available reagents were used as received. Solvents were distilled from relevant drying agents prior to use. 3,3-Dialkyl-3,4-dihydro-2*H*-thieno[3,4-*b*][1,4]dioxepine (ProDOT-R),[54] 2,2′,3,3′-tetrahydro-5,5′-bithieno[3,4-*b*]-1,4-dioxin (EDOT dimer),[55] and 3,3,3′,3′-tetraethyl-3,3′,4,4′-tetrahydro-6,6′-bi-2*H*-thieno[3,4-*b*][1,4]-dioxepin (ProDOT-Et dimer)[56] were prepared according to the literature procedures.

Computational Methods. DFT calculations were performed with the Gaussian 09 (Revision D.01) program.[57] Geometry optimizations were carried out using pruned (99,590) grids (by Int = UltraFine keyword) with solvation of dichloromethane based on the polarizable continuum model (PCM) as implemented in Gaussian 09. Frequency calculations were conducted after geometry optimizations. Some structures were found to show small imaginary frequencies, which are considered most likely to be an artifact of the calculation.[58,59] As concerns the methylene-oxy parts in the propylene dioxy moiety of the ProDOT unit in $(\mathbf{3P_{Me}})_2^{2+}$, the optimized conformer with all the methylene parts pointing inside the dimer structure at the RB97D3/6-31G(d) level (Figure S5a) was shown to be 15.2 kcal mol^{-1} less stable than the structure with all pointing outside (Figure S5b). Therefore, the corresponding conformation with the parts pointing outside was also applied to the ProDOT units of $(\mathbf{2E2P_{Me}})_2^{2+}$ and $(\mathbf{2E3P_{Me}})_2^{2+}$. For $(\mathbf{2E2P_{Me}})_2^{2+}$, both "head-to-tail" and "head-to-head" (Figure S5c) structures were optimized and the head-to-head dimer was found to be 0.32 kcal mol^{-1} less stable probably due to the steric repulsion between neighboring ProDOT units. Thus, only the head-to-tail dimer was optimized for $(\mathbf{2E3P_{Me}})_2^{2+}$. Excitation energy was computed using time-dependent density functional theory (TD-DFT) using the optimized geometry at the same DFT level and basis set. The calculated π-dimerization energy ΔE_{dim} was obtained from the total energies of the radical cation monomer and the π-dimer.

Synthesis of 1. To a solution of ProDOT-Me (660 mg, 3.58 mmol) in THF (12 mL) was added *n*-butyllithium (2.8 mL, 4.2 mmol) in hexane at −80 °C under N_2. After stirring for 2 h, dimethyldisulfide (1.6 mL, 18 mmol) was added dropwise to the reaction mixture and then allowed to warm to room temperature. After stirring for 3 h, water was added and the mixture was extracted with ether and dried over $MgSO_4$. After removal of volatiles in vacuo, the reaction mixture was purified by a short column chromatography (SiO_2) using hexane/ethyl acetate (25:1) as eluent to give **1** (pale yellow oil, 789 mg, 3.43 mmol, 96% yield); ^{1}H NMR (270 MHz, $CDCl_3$) δ 6.49 (s, 1H), 3.83 (s, 2H), 3.74 (s, 2H), 2.37 (s, 3H), 1.04 (s, 6H); ^{13}C NMR (67.5 MHz, $CDCl_3$) δ 150.9, 149.4, 114.7, 106.7, 80.0, 79.9, 38.9, 21.6, 21.2; HRMS (APCI-TOF) calcd for $C_{10}H_{15}O_2S_2$ [(M + H)$^+$] = 231.0513; found 231.0485.

Synthesis of 2. To a mixture of ProDOT-Me (600 mg, 3.26 mmol) and *N*-iodosuccinimide (1.46 g, 6.49 mmol) was added DMF (40 mL) at rt under N_2. After stirring overnight, water was added and the mixture was extracted with ether and dried over $MgSO_4$. After removal of volatiles in vacuo, the reaction mixture was passed through a short column chromatography (SiO_2) using hexane/dichloromethane (10:1) as eluent to give **2** (1.12 g, 2.57 mmol, 79% yield). Recrystallization from hot acetone gave colorless crystals: mp 147−149 °C; ^{1}H NMR (270 MHz, C_6D_6) δ 3.16 (s, 4H), 0.50 (s, 6H); ^{13}C NMR (67.5 MHz, C_6D_6) δ 151.7, 79.7, 60.0, 38.3, 21.3; HRMS (APCI-TOF) calcd for $C_9H_{10}I_2O_2S$ [(M)$^+$] = 435.8491; found 435.8461.

Synthesis of $\mathbf{3P_{Me}}$. To a THF solution (15 mL) of **1** (1.05 g, 4.56 mmol) was added *n*-butyllithium (3.75 mL, 5.77 mmol) in hexane at −80 °C under N_2. After stirring for 3 h at −80 °C, trimethyltin chloride (5.77 mL, 5.77 mmol) in dichloromethane was added and then allowed to warm to room temperature. After stirring overnight, the volatiles were removed in vacuo and the residue was passed through a pad of Celite with hexane, which gave crude stannylated **1** (1.80 g) as a yellow oil. To the crude stannylated derivative of **1** (1.3 g), **2** (431 mg, 0.988 mmol), and $Pd(PPh_3)_4$ (230 mg, 0.20 mmol) was added toluene (30 mL) under N_2. After refluxed overnight, volatiles were removed in vacuo, and the reaction mixture was passed through a short column chromatography (Al_2O_3) using hexane/dichloromethane (v/v = 2:1) as eluent. After evaporation, the residue was separated by preparative GPC eluted with toluene to give $\mathbf{3P_{Me}}$ (209 mg, 0.326 mmol, 33%) as a yellow solid: mp > 220 °C (dec.); ^{1}H NMR (500 MHz, C_6D_6) δ 3.55 (s, 4H), 3.44 (s, 4H), 3.40 (s, 4H), 2.20 (s, 6H), 0.70 (s, 6H), 0.67 (s, 12H); ^{13}C NMR (125 MHz, C_6D_6) δ 151.7, 146.3, 145.6, 118.0, 114.6, 113.9, 80.2, 80.1, 80.0, 38.7, 21.3, 21.2, 20.9; HRMS (APCI-TOF) calcd for $C_{29}H_{36}O_6S_5$ [(M)$^+$] = 640.1115; found 640.1100.

Synthesis of 3. To a solution of EDOT dimer (1.00 g, 3.54 mmol) in THF (35 mL) was added *n*-butyllithium (2.66 mL, 4.25 mmol) in hexane at −80 °C under N_2. After stirring for 2 h, dimethyldisulfide (1.6 mL, 18 mmol) was added dropwise to the reaction mixture and then allowed to warm to room temperature. After stirring for 3 h, water was added and the mixture was extracted with ether and dried over $MgSO_4$. After removal of the solvent in vacuo, the reaction mixture was passed through a short column chromatography (SiO_2 deactivated with 10% water) using dichloromethane as eluent. After evaporation, the residue was separated by preparative GPC eluted with chloroform to give **3** (928 mg, 2.83 mmol, 80% yield). Recrystallization from hot ethanol gave pale yellow needle crystals: mp 160−161 °C; ^{1}H NMR (500 MHz, $CDCl_3$) δ 6.28 (s, 1H), 4.33 (m, 2H), 4.32 (s, 4H), 4.24 (m, 2H), 2.38 (s, 3H); ^{13}C NMR (125 MHz, $CDCl_3$) δ 142.8, 141.2, 137.4, 136.3, 112.2, 109.5, 106.2, 98.0, 65.04, 64.96, 64.7, 64.6, 21.4; HRMS (APCI-TOF) calcd for $C_{13}H_{12}O_4S_3$ [(M)$^+$] = 327.9898; found 327.9889.

Synthesis of 4. To a solution of ProDOT-Et dimer (1.00 g, 2.37 mmol) in THF (30 mL) was added *n*-butyllithium (1.7 mL, 2.8 mmol) in hexane at −80 °C under N_2. After stirring for 2 h, dimethyldisulfide (2.1 mL, 24 mmol) in THF was added dropwise to the reaction mixture and then allowed to warm to room temperature. After stirring overnight, water was added and the mixture was extracted with ether and dried over $MgSO_4$. After removal of the solvent in vacuo, the

DOI: 10.1021/acs.joc.7b00816
J. Org. Chem. 2017, 82, 7245−7253

reaction mixture was passed through a short column chromatography (SiO_2 deactivated with 10% water) using hexane/dichloromethane (3:1) as eluent. After evaporation, the residue was separated by preparative GPC eluted with toluene to give **4** (pale yellow oil, 605 mg, 1.29 mmol, 54% yield) ; ^{1}H NMR (270 MHz, C_6D_6) δ 6.32 (s, 1H), 3.68 (s, 2H), 3.66 (s, 2H), 3.58 (s, 2H), 3.57 (s, 2H), 2.19 (s, 3H), 1.50 (m. 8H), 0.58 (m, 12H); ^{13}C NMR (67.5 MHz, C_6D_6) δ 151.3, 150.0, 146.1, 145.2, 117.2, 115.4, 112.1, 103.2, 77.2, 77.0, 43.77, 43.74, 23.75, 23.67, 21.1, 7.27, 7.29; HRMS (APCI-TOF) calcd for $C_{23}H_{32}O_4S_3$ [$(M)^+$] = 468.1463; found 468.1442.

Synthesis of 2E2P$_{Et}$. To a solution of **3** (790 mg, 2.41 mmol) in THF (24 mL) was added *n*-butyllithium (2.26 mL, 3.61 mmol) in hexane at −80 °C under N_2. After stirring for 2 h, tributyltin chloride (1.04 mL, 3.84 mmol) was added dropwise to the reaction mixture and then allowed to warm to room temperature. After stirring for 2 h, volatiles were removed in vacuo and the reaction mixture was passed through a pad of Celite using hexane as eluent. After removal of hexane under reduced pressure, the residue including stannylated **3** (**3-*Sn***) was separated by preparative GPC eluted with toluene to give a waxy yellow solid (crude yield 75%).

To a dichloromethane solution (10 mL) of **4** (75 mg, 0.16 mmol) was added pyridinium iodochloride (42 mg, 0.17 mmol) at rt under N_2. After stirring for 2 h, volatiles were removed in vacuo. Flash column chromatography (SiO_2 deactivated with 10% water) using hexane/dichloromethane (4:3) as eluent gave crude iodinated **4**(**4-*I*** 78 mg 87%, determined by ^{1}H NMR) as a dark brown solid. To the crude **3-*Sn*** (65 mg, 0.10 mmol), **4-*I*** (75 mg, 0.13 mmol), and $Pd(PPh_3)_4$ (30 mg, 0.027 mmol) was added toluene (10 mL) under N_2. After refluxed overnight, volatiles were removed in vacuo, and the residue was passed through a short column chromatography (Al_2O_3) using hexane/dichloromethane (3:1) as eluent. After evaporation, the residue was separated by preparative GPC eluted with toluene to give **2E2P$_{Et}$** (20 mg, 0.026 mmol, 26%) as an orange solid: mp > 236 °C (dec.); ^{1}H NMR (500 MHz, C_6D_6) δ 3.745 (s, 2H), 3.737 (s, 2H), 3.68 (s, 2H), 3.60 (s, 2H), 3.44 (m, 6H), 3.36(m, 2H), 2.21 (s, 3H), 2.15 (s, 3H), 1.2 (m, 8H) 0.60 (m, 12H); ^{13}C NMR (125 MHz, C_6D_6) δ 151.4, 146.2, 145.2, 145.1, 143.5, 137.9, 137.7, 137.0, 117.4, 114.2, 113.7, 113.1, 112.36, 110.0, 109.3, 107.2, 77.8, 77.7, 77.2, 77.0, 64.8, 64.5, 64.3, 43.7, 43.7, 23.7, 21.0, 7.3; HRMS (APCI-TOF) calcd for $C_{36}H_{42}O_8S_6$ [$(M)^+$] = 794.1204; found 794.1215.

Synthesis of 5. To a THF solution (15 mL) of ProDOT-Et (1.00 g, 4.71 mmol) was added *n*-butyllithium (3.4 mL, 5.65 mmol) in hexane at −80 °C under N_2. After stirring for 2 h at −80 °C, trimethyltin chloride (1.0 M, 5.7 mmol) in dichloromethane was added and then allowed to warm to room temperature. After stirring 3 h, volatiles were removed in vacuo and the reaction mixture was passed through a pad of Celite using hexane as eluent. After removal of hexane under reduced pressure, the residue including stannylated ProDOT-Et was separated by preparative GPC eluted with toluene to give a pale yellow oil. To a mixture of crude stannylated ProDOT-Et (158 mg, 0.44 mmol), crude **4-*I*** (225 mg, 0.40 mmol), and $Pd(PPh_3)_4$ (92 mg, 0.08 mmol) was added toluene (20 mL) under N_2. After refluxed overnight, volatiles were removed in vacuo, and the residue was passed through a short column chromatography (Al_2O_3) using hexane/dichloromethane (3:1) as eluent. After evaporation, the residue was separated by preparative GPC eluted with toluene to give **5** (90 mg, 0.13 mmol, 33%) as a yellow oil: ^{1}H NMR (270 MHz, C_6D_6) δ 6.36 (s, 1H), 3.77 (s, 2H), 3.74 (s, 2H), 3.68 (s, 4H), 3.60 (s, 4H), 2.20 (s, 3H), 1.2 (m, 12H) 0.6 (m, 18H); ^{13}C NMR (67.5 MHz, C_6D_6) δ 151.4, 150.1, 146.0, 145.8, 145.6, 143.1, 117.3, 115.9, 114.3, 113.5, 112.4, 103.4, 77.3, 77.2, 76.92, 76.89, 43.7, 43.7, 23.8, 23.6, 21.1, 7.30, 7.28; 9; HRMS (APCI-TOF) calcd for $C_{34}H_{46}O_6S_4$ [$(M)^+$] = 678.2177; found 678.2177.

Synthesis of 2E3P$_{Et}$. To a THF solution (10 mL) of **5** (150 mg, 0.22 mmol) was added *n*-butyllithium (1.6 M, 0.24 mmol) in hexane at −80 °C under N_2. After stirring for 2 h at −80 °C, iodine (62 mg, 0.24 mmol) in THF was added and then allowed to warm to room temperature. After stirring overnight, the reaction mixture was quenched with $Na_2S_2O_3$ and the mixture was extracted with ether. The organic layer was washed with brine and dried over Na_2SO_4. Removal of the solvent in vacuo gave crude iodinated **5** (**5-*I***: 88%, determined by NMR) as a dark yellow oil. To crude **3-*Sn*** (95 mg, 0.15 mmol), **5-*I*** (168 mg, 0.18 mmol), and $Pd(PPh_3)_4$ (43.9 mg, 0.038 mmol) was added toluene (15 mL) under N_2. After refluxed overnight, the reaction mixture was quenched with water and the mixture was extracted with ether and dried over Na_2SO_4. After removal of the solvent in vacuo, the reaction mixture was passed through a short column chromatography (Al_2O_3) using hexane/dichloromethane (v/v = 3:2) as eluent. After evaporation, the residue was separated by preparative GPC eluted with toluene to give **2E3P$_{Et}$** (72 mg, 0.072 mmol, 48%) as an orange solid: mp > 240 °C (dec.); ^{1}H NMR (500 MHz, C_6D_6) δ 3.782 (s, 2H), 3.776 (s, 2H), 3.765 (s, 2H), 3.75 (s, 2H), 3.69 (s, 2H), 3.46 (m, 6H), 3.38(m, 4H), 2.21 (s, 3H), 2.16 (s, 3H), 1.1−1.3 (m, 12H), 0.60 (m, 18H); ^{13}C NMR (125 MHz, C_6D_6) δ 151.6, 146.2, 145.9, 145.5, 145.4, 145.2, 143.6, 138.0, 137.7, 137.0, 117.5, 114.7, 114.4, 114.3, 113.9, 113.2, 112.4, 110.2, 109.2, 107.2, 77.84, 77.80, 77.3, 77.0, 64.8, 64.7, 64.6, 64.4, 43.8, 43.7, 23.7, 21.11, 21.10, 7.34, 7.28; HRMS (APCI-TOF) calcd for $C_{47}H_{56}O_{10}S_7$ [$(M)^+$] = 1004.1918; found 1004.1969.

■ ASSOCIATED CONTENT

Supporting Information

The Supporting Information is available free of charge on the ACS Publications website at DOI: 10.1021/acs.joc.7b00816.

^{1}H and ^{13}C NMR spectra; Figures S1−S5; Cartesian coordinates and total energies of the optimized structures of all calculated molecules (PDF)

■ AUTHOR INFORMATION

Corresponding Author

*E-mail: nishinaga-tohru@tmu.ac.jp.

ORCID

Tohru Nishinaga: 0000-0002-9081-3659

Notes

The authors declare no competing financial interest.

■ ACKNOWLEDGMENTS

We are grateful to Prof. Kotohiro Nomura for his encouragements. This work was supported by a Grant-in-Aid for Scientific Research on Innovative Areas (15H00954).

■ REFERENCES

(1) Kahlfuss, C.; Saint-Aman, E.; Bucher, C. In *Organic Redox Systems: Synthesis, Properties, and Applications*; Nishinaga, T., Ed.; Wiley: Hoboken. NJ, 2016; pp 39−88.

(2) Zhang, D. W.; Tian, J.; Chen, L.; Zhang, L.; Li, Z. T. *Chem. - Asian J.* **2015**, *10*, 56−68.

(3) Preuss, K. E. *Polyhedron* **2014**, *79*, 1−15.

(4) Nishinaga, T.; Komatsu, K. *Org. Biomol. Chem.* **2005**, *3*, 561−569.

(5) Trabolsi, A.; Khashab, N.; Fahrenbach, A. C.; Friedman, D. C.; Colvin, M. T.; Cotí, K. K.; Benítez, D.; Tkatchouk, E.; Olsen, J.-C.; Belowich, M. E.; Carmielli, R.; Khatib, H. A.; Goddard, W. A.; Wasielewski, M. R.; Stoddart, J. F. *Nat. Chem.* **2010**, *2*, 42−49.

(6) Iordache, A.; Oltean, M.; Milet, A.; Thomas, F.; Baptiste, B.; Saint-Aman, E.; Bucher, C. *J. Am. Chem. Soc.* **2012**, *134*, 2653−2671.

(7) Fahrenbach, A. C.; Zhu, Z.; Cao, D.; Liu, W. G.; Li, H.; Dey, S. K.; Basu, S.; Trabolsi, A.; Botros, Y. Y.; Goddard, W. A.; Stoddart, J. F. *J. Am. Chem. Soc.* **2012**, *134*, 16275−16288.

(8) Barnes, J. C.; Fahrenbach, A. C.; Cao, D.; Dyar, S. M.; Frasconi, M.; Giesener, M. A.; Benítez, D.; Tkatchouk, E.; Chernyashevskyy, O.; Shin, W. H.; Li, H.; Sampath, S.; Stern, C. L.; Sarjeant, A. A.; Hartlieb, K. J.; Liu, Z.; Carmieli, R.; Botros, Y. Y.; Choi, J. W.; Slawin, A. M. Z.; Ketterson, J. B.; Wasielewski, M. R.; Goddard, W. A.; Stoddart, J. F. *Science* **2013**, *339*, 429−433.

DOI: 10.1021/acs.joc.7b00816
J. Org. Chem. 2017, 82, 7245−7253

(9) Bruns, C. J.; Frasconi, M.; Iehl, J.; Hartlieb, K. J.; Schneebeli, S. T.; Cheng, C.; Stupp, S. I.; Stoddart, J. F. *J. Am. Chem. Soc.* **2014**, *136*, 4714−4723.
(10) Wang, Y.; Frasconi, M.; Liu, W. G.; Liu, Z.; Sarjeant, A. A.; Nassar, M. S.; Botros, Y. Y.; Goddard, W. A.; Stoddart, J. F. *J. Am. Chem. Soc.* **2015**, *137*, 876−885.
(11) Zhou, C.; Tian, J.; Wang, J.-L.; Zhang, D.-W.; Zhao, X.; Liu, Y.; Li, Z.-T. *Polym. Chem.* **2014**, *5*, 341−345.
(12) Spruell, J. M.; Coskun, A.; Friedman, D. C.; Forgan, R. S.; Sarjeant, A. a; Trabolsi, A.; Fahrenbach, A. C.; Barin, G.; Paxton, W. F.; Dey, S. K.; Olson, M. a; Benítez, D.; Tkatchouk, E.; Colvin, M. T.; Carmielli, R.; Caldwell, S. T.; Rosair, G. M.; Hewage, S. G.; Duclairoir, F.; Seymour, J. L.; Slawin, A. M. Z.; Goddard, W. a; Wasielewski, M. R.; Cooke, G.; Stoddart, J. F. *Nat. Chem.* **2010**, *2*, 870−879.
(13) Coskun, A.; Spruell, J. M.; Barin, G.; Fahrenbach, A. C.; Forgan, R. S.; Colvin, M. T.; Carmieli, R.; Benítez, D.; Tkatchouk, E.; Friedman, D. C.; Sarjeant, A. A.; Wasielewski, M. R.; Goddard, W. A.; Stoddart, J. F. *J. Am. Chem. Soc.* **2011**, *133*, 4538−4547.
(14) Tian, J.; Ding, Y.-D.; Zhou, T.-Y.; Zhang, K.-D.; Zhao, X.; Wang, H.; Zhang, D.-W.; Liu, Y.; Li, Z.-T. *Chem. - Eur. J.* **2014**, *20*, 575−584.
(15) Nishinaga, T. In *Organic Redox Systems: Synthesis, Properties, and Applications*; Nishinaga, T., Ed.; Wiley: Hoboken, NJ, 2016; pp 383−410.
(16) Apperloo, J. J.; Janssen, R. A. J.; Malenfant, P. R. L.; Groenendaal, L.; Fréchet, J. M. J. *J. Am. Chem. Soc.* **2000**, *122*, 7042−7051.
(17) Song, C.; Swager, T. M. *Org. Lett.* **2008**, *10*, 3575−3578.
(18) Tateno, M.; Takase, M.; Nishinaga, T. *Chem. Mater.* **2014**, *26*, 3804−3810.
(19) Takai, A.; Yasuda, T.; Ishizuka, T.; Kojima, T.; Takeuchi, M. *Angew. Chem., Int. Ed.* **2013**, *52*, 9167−9171.
(20) Miller, L. L.; Mann, K. R. *Acc. Chem. Res.* **1996**, *29*, 417−423.
(21) Hill, M. G.; Mann, K. R.; Miller, L. L.; Penneau, J.-F. *J. Am. Chem. Soc.* **1992**, *114*, 2728−2730.
(22) Bäuerle, P.; Segelbacher, U.; Maier, A.; Mehring, M. *J. Am. Chem. Soc.* **1993**, *115*, 10217−10223.
(23) Graf, D. D.; Duan, R. G.; Campbell, J. P.; Miller, L. L.; Mann, K. R. *J. Am. Chem. Soc.* **1997**, *119*, 5888−5899.
(24) Levillain, E.; Roncali, J. *J. Am. Chem. Soc.* **1999**, *121*, 8760−8765.
(25) Apperloo, J.; Raimundo, J.; Frere, P.; Roncali, J.; Janssen, R. *Chem. - Eur. J.* **2000**, *6*, 1698−1707.
(26) Sakai, T.; Satou, T.; Kaikawa, T.; Takimiya, K.; Otsubo, T.; Aso, Y. *J. Am. Chem. Soc.* **2005**, *127*, 8082−8089.
(27) Knoblock, K. M.; Silvestri, C. J.; Collard, D. M. *J. Am. Chem. Soc.* **2006**, *128*, 13680−13681.
(28) Casado, J.; Takimiya, K.; Otsubo, T.; Ramírez, F. J.; Quirante, J. J.; Ponce Ortiz, R.; González, S. R.; Moreno Oliva, M.; López Navarrete, J. T. *J. Am. Chem. Soc.* **2008**, *130*, 14028−14029.
(29) Malavé Osuna, R.; Ruiz Delgado, M. C.; Hernández, V.; López Navarrete, J. T.; Vercelli, B.; Zotti, G.; Novoa, J. J.; Suzuki, Y.; Yamaguchi, S.; Henssler, J. T.; Matzger, A. J. *Chem. - Eur. J.* **2009**, *15*, 12346−12361.
(30) Chen, X.; Ma, B.; Chen, S.; Li, Y.; Huang, W.; Ma, J.; Wang, X. *Chem. - Asian J.* **2013**, *8*, 238−243.
(31) Ferrón, C. C.; Capdevila-Cortada, M.; Balster, R.; Hartl, F.; Niu, W.; He, M.; Novoa, J. J.; López Navarrete, J. T.; Hernández, V.; Ruizdelgado, M. C. *Chem. - Eur. J.* **2014**, *20*, 10351−10359.
(32) Ie, Y.; Okamoto, Y.; Tone, S.; Aso, Y. *Chem. - Eur. J.* **2015**, *21*, 16688−16695.
(33) Nishinaga, T.; Wakamiya, A.; Yamazaki, D.; Komatsu, K. *J. Am. Chem. Soc.* **2004**, *126*, 3163−3174.
(34) Yamazaki, D.; Nishinaga, T.; Tanino, N.; Komatsu, K. *J. Am. Chem. Soc.* **2006**, *128*, 14470−14471.
(35) Tateno, M.; Takase, M.; Iyoda, M.; Komatsu, K.; Nishinaga, T. *Chem. - Eur. J.* **2013**, *19*, 5457−5467.
(36) Hasegawa, M.; Kobayakawa, K.; Matsuzawa, H.; Nishinaga, T.; Hirose, T.; Sako, K.; Mazaki, Y. *Chem. - Eur. J.* **2017**, *23*, 3267−3271.
(37) Hicks, R. G.; Nodwell, M. B. *J. Am. Chem. Soc.* **2000**, *122*, 6746−6753.
(38) Apperloo, J. J.; Groenendaal, L. B.; Verheyen, H.; Jayakannan, M.; Janssen, R. a J.; Dkhissi, A.; Beljonne, D.; Lazzaroni, R.; Brédas, J.-L. *Chem. - Eur. J.* **2002**, *8*, 2384−2396.
(39) Turbiez, M.; Frère, P.; Roncali, J. *J. Org. Chem.* **2003**, *68*, 5357−5360.
(40) Wasserberg, D.; Meskers, S. C. J.; Janssen, R. A. J.; Mena-Osteritz, E.; Bäuerle, P. *J. Am. Chem. Soc.* **2006**, *128*, 17007−17017.
(41) Burrezo, P. M.; Pelado, B.; Ortiz, R. P.; De la Cruz, P.; Navarrete, J. T. L.; Langa, F.; Casado, J. *Chem. - Eur. J.* **2015**, *21*, 1713−1725.
(42) Kirchmeyer, S.; Reuter, K. *J. Mater. Chem.* **2005**, *15*, 2077.
(43) Amb, C. M.; Dyer, A. L.; Reynolds, J. R. *Chem. Mater.* **2011**, *23*, 397−415.
(44) Lin, C.; Endo, T.; Takase, M.; Iyoda, M.; Nishinaga, T. *J. Am. Chem. Soc.* **2011**, *133*, 11339−11350.
(45) Lü, J.-M.; Rosokha, S. V.; Kochi, J. K. *J. Am. Chem. Soc.* **2003**, *125*, 12161−12171.
(46) Yu, Y.; Gunic, E.; Zinger, B.; Miller, L. L. *J. Am. Chem. Soc.* **1996**, *118*, 1013−1018.
(47) Nishinaga, T.; Kageyama, T.; Koizumi, M.; Ando, K.; Takase, M.; Iyoda, M. *J. Org. Chem.* **2013**, *78*, 9205−9213.
(48) Zhao, Y.; Truhlar, D. G. *Acc. Chem. Res.* **2008**, *41*, 157−167.
(49) Doehnert, D.; Koutecky, J. *J. Am. Chem. Soc.* **1980**, *102*, 1789−1796.
(50) Fumanal, M.; Capdevila-Cortada, M.; Ribas-Arino, J.; Novoa, J. J. *J. Chem. Theory Comput.* **2015**, *11*, 2651−2660.
(51) Beneberu, H. Z.; Tian, Y.-H.; Kertesz, M. *Phys. Chem. Chem. Phys.* **2012**, *14*, 10713−10725.
(52) Capdevila-Cortada, M.; Ribas-Arino, J.; Novoa, J. J. *J. Chem. Theory Comput.* **2014**, *10*, 650−658.
(53) Sherrill, C. D.; Lee, M. S.; Head-Gordon, M. *Chem. Phys. Lett.* **1999**, *302*, 425−430.
(54) Liang, Y.; Peng, B.; Liang, J.; Tao, Z.; Chen, J. *Org. Lett.* **2010**, *12*, 1204−1207.
(55) Swager, T. M.; Kingsborough, R.; Zhu, S. S. U.S. Patent 6,323,309, 2001.
(56) Welsh, D. M.; Kloeppner, L. J.; Madrigal, L.; Pinto, M. R.; Thompson, B. C.; Schanze, K. S.; Abboud, K. A.; Powell, D.; Reynolds, J. R. *Macromolecules* **2002**, *35*, 6517−6525.
(57) Frisch, M. J.; Trucks, G. W.; Schlegel, H. B.; Scuseria, G. E.; Robb, M. A.; Cheeseman, J. R.; Scalmani, G.; Barone, V.; Mennucci, B.; Petersson, G. A.; Nakatsuji, H.; Caricato, M.; Li, X.; Hratchian, H. P.; Izmaylov, A. F.; Bloino, J.; Zheng, G.; Sonnenberg, J. L.; Hada, M.; Ehara, M.; Toyota, K.; Fukuda, R.; Hasegawa, J.; Ishida, M.; Nakajima, T.; Honda, Y.; Kitao, O.; Nakai, H.; Vreven, T.; Montgomery, J. A., Jr.; Peralta, J. E.; Ogliaro, F.; Bearpark, M.; Heyd, J. J.; Brothers, E.; Kudin, K. N.; Staroverov, V. N.; Kobayashi, R.; Normand, J.; Raghavachari, K.; Rendell, A.; Burant, J. C.; Iyengar, S. S.; Tomasi, J.; Cossi, M.; Rega, N.; Millam, J. M.; Klene, M.; Knox, J. E.; Cross, J. B.; Bakken, V.; Adamo, C.; Jaramillo, J.; Gomperts, R.; Stratmann, R. E.; Yazyev, O.; Austin, A. J.; Cammi, R.; Pomelli, C.; Ochterski, J. W.; Martin, R. L.; Morokuma, K.; Zakrzewski, V. G.; Voth, G. A.; Salvador, P.; Dannenberg, J. J.; Dapprich, S.; Daniels, A. D.; Farkas, Ö.; Foresman, J. B.; Ortiz, J. V.; Cioslowski, J.; Fox, D. J. *Gaussian 09*, Revision D.01; Gaussian, Inc.: Wallingford, CT, 2013.
(58) Cobar, E. A.; Khaliullin, R. Z.; Bergman, R. G.; Head-Gordon, M. *Proc. Natl. Acad. Sci. U. S. A.* **2007**, *104*, 6963−6968.
(59) Bialas, D.; Zitzler-Kunkel, A.; Kirchner, E.; Schmidt, D.; Würthner, F. *Nat. Commun.* **2016**, *7*, 12949.

DOI: 10.1021/acs.joc.7b00816
J. Org. Chem. 2017, 82, 7245−7253